A Back-Fire to Forward Wide-Angle Beam Steering Leaky-Wave Antenna Based on SSPPs

Longfang Ye, *Member, IEEE*, Zhengyi Wang, Jianliang Zhuo, *Member, IEEE*, Feng Han, *Senior Member, IEEE*, Weiwen Li, *Senior Member, IEEE*, and Qing Huo Liu, *Fellow, IEEE*

***Abstract*— We demonstrate an efficient back-fire to forward wide-angle beam steering leaky-wave antenna (LWA) based on a large dispersion gradient planar spoof surface plasmon polariton (SSPP) transmission line (TL) with split-ring units. To convert the highly confined SSPP waveguiding mode to a radiation mode, two arrays of metallic patches are periodically arranged on both sides of the SSPP TL. The patches are designed as two combined half-elliptical shapes to mitigate the open stopband effect and enhance the radiation performance. We propose a theoretical method to interpret the mechanism and predict the directional pattern of the LWA. To verify the proposed method, the SSPP TL and LWA prototypes are fabricated and measured. The calculation, simulation, and experimental results match well and show that the main beam of the LWA can steer a wide range of 112° from back-fire (−90°) to the forward quadrant of 22° passing through the broadside in 6.3–11 GHz, demonstrating a large scanning rate of 2.07°/%. Furthermore, the LWA also possesses the advantages of low profile, high average gain (12 dBi), high average efficiency (95%), and low sidelobe level (<−13 dB). This work provides an alternative route to achieving wide-angle LWAs for promising microwave radar and wireless communication applications.**

***Index Terms*— Beam steering, leaky-wave antenna (LWA), spoof surface plasmon polaritons (SSPPs).**

I. Introduction

FREQUENCY beam-scanning antennas have been studied extensively owing to the scanning beam characteristics enabled by the sweeping frequency, which have been widely applied in microwave radar and wireless communication systems. As one type of frequency beam-scanning antennas, leaky-wave antennas (LWAs) have gained increasing attention in recent years. LWAs usually generate leaky-wave radiations by leaking the electromagnetic (EM) energy gradually along with the structures [1], possessing great capabilities in main beam manipulation and steering. The early leaky-wave structures were realized on periodically slotted rectangular waveguides [2]. Generally, LWAs have two typical structures: the uniform and periodic structures [3]. The slotted rectangular waveguide is one of the simplest traditional uniform LWAs, which can only scan its main beam in the forward quadrant space. The LWAs with periodic structures such as periodically loaded dielectric waveguides, impedance modulated microstrips, composite right/left-hand (CRLH) transmission lines (TLs) can scan both in forward and backward quadrant space. For example, a number of LWAs based on periodic half-width microstrips [4], coupled half-width microstrips [5], substrate-integrated waveguides (SIWs) with period gaps [6], [7], CRLH waveguides [8], and asymmetrically modulated Goubau Line [9], [10] with high-efficiency wide-angle scanning capability have been demonstrated. However, many previously proposed LWAs suffer from a limited scanning range in a given narrow operating band and drastic degradation around the broadside, namely the "open stop band" (OSB) effects [3].

The scanning range of an LWA is mainly dependent on the dispersion relations of the TLs. To increase the scanning range in a narrow band, many slow-wave spoof surface plasmon polariton (SSPP) TLs with large gradient dispersion relations were introduced into the LWA designs [11], [12]. SSPPs are one variety of surface EM waves propagating along decorated metallic surfaces at microwave and terahertz frequencies, whose dispersion characteristics are similar to surface plasmon polaritons (SPPs) in the optical region [13]–[16]. Recently, a lot of SSPP TLs based on bulk and planar structures have been proposed for high-efficiency SSPP propagation [17]. Owing to the advantages of smaller size, stronger confinement, and easier fabrication, the corrugated ultrathin metallic SSPP waveguides have attracted extensive attention. These TLs provide a new way to achieve many versatile planar plasmonic integrated devices and circuits such as SSPP filters, amplifiers, couplers, splitters, and antennas in microwave and terahertz regimes [18]–[26]. Owing to the strong slow-wave dispersion characteristics of SSPPs, the SSPP-based LWAs usually show high scanning rates, namely the scanning range divided by the relative bandwidth (°/%) [27], [28]. To convert the bounded SSPP mode to radiation mode, the slow-wave SSPPs along the

Manuscript received March 5, 2021; revised November 6, 2021; accepted November 11, 2021. Date of publication January 4, 2022; date of current version May 5, 2022. This work was supported in part by the Shenzhen Science and Technology Projects under Grant JCYJ20180306172733197 and Grant JCYJ20210324121606017, in part by the State Key Laboratory of Millimeter Waves under Grant K202101, and in part by the Fundamental Research Funds for the Central Universities under Grant 20720210048. *(Corresponding author: Longfang Ye.)*

Longfang Ye is with the Institute of Electromagnetics and Acoustics, Xiamen University, Xiamen 361005, China, also with the Shenzhen Research Institute, Xiamen University, Shenzhen 518057, China, and also with the State Key Laboratory of Millimeter Waves, Southeast University, Nanjing 210096, China (e-mail: lfye@xmu.edu.cn).

Zhengyi Wang, Jianliang Zhuo, and Feng Han are with the Institute of Electromagnetics and Acoustics, Xiamen University, Xiamen 361005, China.

Weiwen Li is with the Department of Electronic Engineering, Xiamen University, Xiamen 361005, China.

Qing Huo Liu is with the Department of Electrical and Computer Engineering, Duke University, Durham, NC 27708 USA.

Color versions of one or more figures in this article are available at https://doi.org/10.1109/TAP.2021.3137241.

Digital Object Identifier 10.1109/TAP.2021.3137241

SSPP TLs should be converted to fast wave mode with $k < k_0$ via periodic impedance modulation or patch array integration. Recently, various SSPP LWAs have been proposed and studied for their high radiation efficiency and wide scanning angle.

In 2015, Xu *et al.* [29] proposed an SSPP emitter with a 1-D phase-gradient metasurface to achieve surface-plasmon-like modes to spatial radiated mode conversion. In 2016, Kong *et al.* [30] proposed an LWA using a sinusoidally modulated SSPP TL based on nonuniform corrugated metallic strips with the scanning range steering from the backward to the forward quadrant. SSPP LWAs with single or double array of circularly metallic patches were presented in [11] and [31]. In 2019, Du *et al.* [32] proposed a wideband LWA using the odd-mode SSPP fish-bone structure for end-fire radiation. Ma *et al.* [33] proposed a compact high-gain LWA based on microstrip SSPPs and substrate integrated waveguide TE_{220} mode. Han *et al.* [34] proposed an LWA based on hybridization of the quasi-TEM mode and SSPP mode to obtain linear frequency steer characteristics. In 2020, Jiang *et al.* [35] proposed an LWA using inductive and capacitive meander-line to achieve a consistent gain in the whole operation band. Another wide-angle LWA combined SSPPs with substrate-integrated waveguide was demonstrated in [28] and [36] to achieve better broadside radiation efficiency. Moreover, wide-angle and circularly polarized LWAs based on double-layer structures with the top layer radiating patches fed by the bottom microstrip SSPP TLs [37], [38] were also demonstrated. In 2021, Zhu *et al.* [39] proposed a kind of patch-loaded SSPP LWAs. However, despite the recent progress, how to design high-performance SSPP LWAs with a wider scanning range, larger scanning rate, higher radiation efficiency, as well as better OSB effect suppression remains a fundamental challenge.

In this article, we proposed an efficient back-fire to forward wide-angle beam steering LWA based on SSPPs. The LWA is composed of a low dispersion asymptotic frequency split ring-shaped SSPP TL and two combined half-elliptical-shaped metallic patch arrays on both sides, enabling the high scanning rate and OSB effect suppression. To investigate the proposed LWA design, we proposed a theoretical method and carried out numerical simulation and experimental verification. The results show that the proposed LWA has excellent radiation performances with a wide scanning range of 112°, an average gain of 12 dBi, an average efficiency of 95% in frequency band 6.3–11 GHz, as well as good OSB effect suppression. Benefit from the larger gradient dispersion relations of the split ring unit, the scanning rate of the proposed SSPP LWA reaches 2.07°/%, which is much higher than many previously reported designs. The proposed SSPP LWA may find some applications in microwave radar and wireless communication systems.

II. Design and Principle

The proposed SSPP LWA is composed of an ultra-thin metallic split-ring-unit-based planar SSPP TL loaded with two arrays of metallic patches on a flexible dielectric substrate, as illustrated in Fig. 1. The metallic layer and the dielectric substrate are copper with a conductivity of 5.8×10^7 S/m and Rogers RT 5880 with a permittivity (ε_r) of 2.2 and loss tangent of 0.0009. The thicknesses of the metallic layer and the substrate are 0.018 and 0.508 mm, and the length and width of the whole antenna are set as $L = 300$ mm and $W = 30$ mm, respectively. In this design, the antenna structure is composed of three sections, Section A, Section B, and Section C, respectively. In Sections A and C, the microstrip-SSPP transitions are made up of a tapered defected ground structure (DGS) and a series of gradually graded-length split-ring SSPP unit cells (seven units) to achieve smooth wave-vector matching and efficient mode-conversion between the quasi-TEM mode of the microstrip and the SSPP mode of SSPP TL. The length and width of the microstrip are set as l_m and w, and the curve function of the DGS is designed as $f(x) = q \cdot (e^{xc/l_g} - 1)/(e^c - 1)$ [40], where q, l_g, and c are the height, length, and curvature, respectively. In Section B, the uniform SSPP TL surrounding by two periodically arranged metallic patch arrays severs as the major radiation section of the LWA, where most of the EM energy is radiated from this area. The patches are designed as two combined half-elliptical shapes with one identical x-axial radius r_x, and two y-axial radiuses r_{y1} and r_{y2} to mitigate the open stopband (OSB) effect and enhance the radiation performance. Two patch arrays distribute periodically on both sides of the SSPP TL with the period p and an x-axial offset a to adjust the far-field pattern of the antenna. The gap between the top of the SSPP TL and the bottom of the patch along the y-axis is g. The detailed dimension parameters of the antenna are shown in Table I.

TABLE I
Dimension Parameters of the Proposed LWA

Parameters	Value	Parameters	Value
W	30	r_{y1}	8.3
L	300	r_{y2}	2.8
l	28.08	r_x	4.7
l_m	10	r_1	0.8
l_g	18.08	r_2	0.533
q	15	w_{stub}	0.266
w	1.574	p_0	2
a	10	Φ	15°
p	20	h_{stub}	0.266
c	2.8	g	0.375

Units: mm.

The radiation principle of the LWA is based on the generation of radiating space harmonics. According to Floquet theory, periodic perturbations on the infinite length SSPP TL can introduce infinite space harmonics of the guided SSPPs waves. If the TL attenuation is ignored, the EM waves in different TL periods only have phase differences. Here, we assume the EM waves propagate along the SSPP TL in the x-direction. The electric field distributions in the first TL period can be expressed as $E(x)$, then the E-field in the second period can be written as $E(x)e^{-j\beta_x p}$, where β_x is the propagation constant in the TL and p is the period of the metallic patch perturbation. Based on this, we can write the propagation constant of these space harmonics as

$$\beta_m = \beta_x + \frac{2m\pi}{p} (m = 0, \pm 1, \pm 2, \ldots\ldots). \tag{1}$$

Although the fundamental mode of the SSPP TL is a slow wave ($\beta_x > k_0$, where k_0 is the propagation constant in free

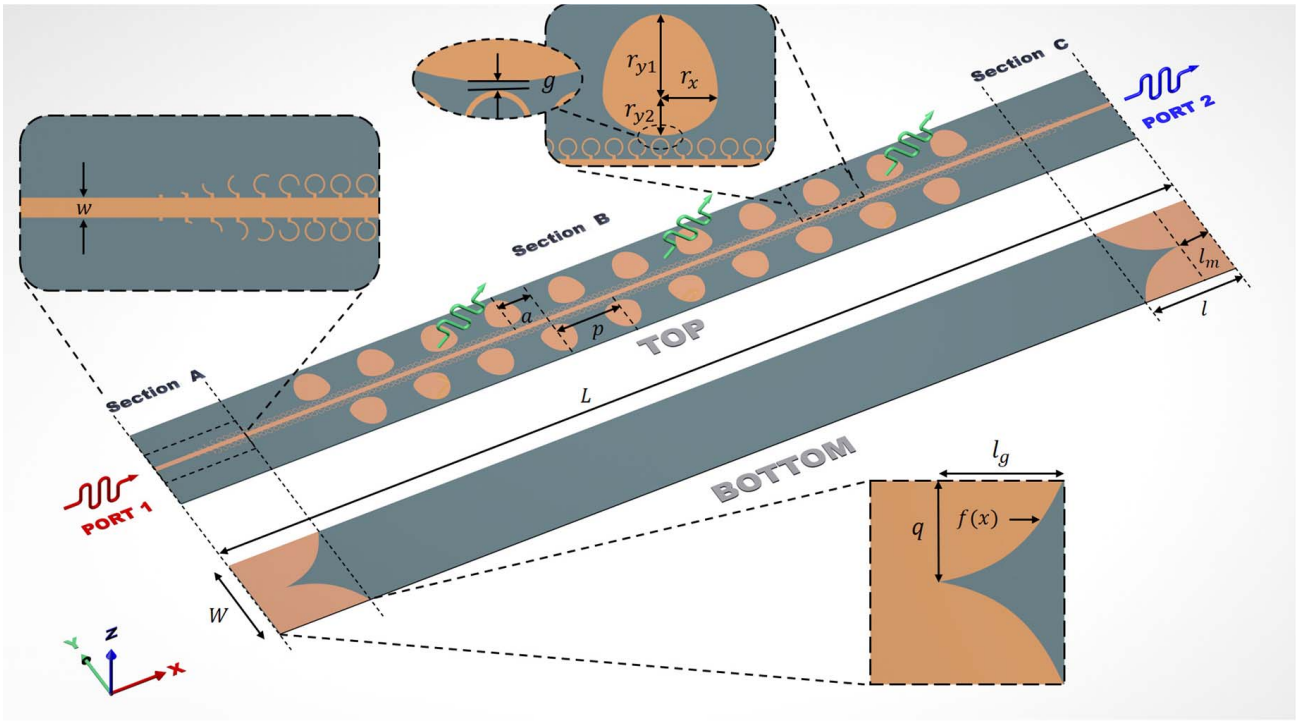

Fig. 1. Schematic diagrams of the proposed antenna. The detailed dimension parameters are listed in Table I.

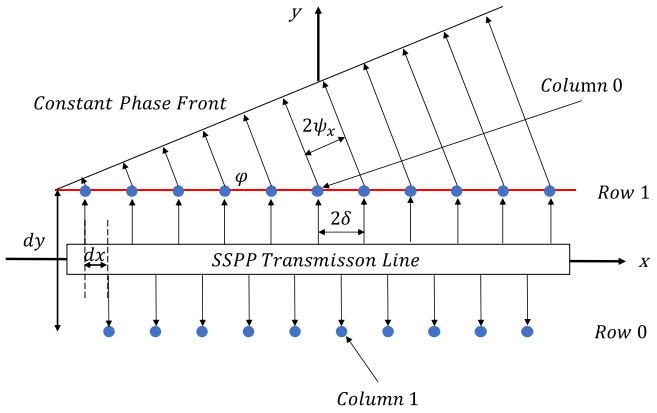

Fig. 2. Equivalent model of the proposed SSPP-based LWA.

space), by choosing a proper p, the negative harmonic modes ($m < 0$) can become fast waves ($\beta_m < k_0$) radiating into the free space. In order to achieve the high radiation efficiency, the $m = -1$ harmonic mode with $-k_0 < \beta_{-1} < k_0$ is selected for the LWA to excite leaky-wave radiation. Then, the main beam direction can be approximately calculated by

$$\theta = \sin^{-1}\left(\frac{\beta_{-1}}{k_0}\right). \tag{2}$$

The metallic patches are designed as the radiating elements of LWA fed by guided waves on the SSPP TL. To facilitate analysis, an equivalent model of the proposed SSPP LWA is plotted in Fig. 2. The directional pattern of a similar non-isotropic point source array is the product of the individual source directional pattern and the isotropic point source array directional pattern with the same position, relative amplitude, and phase. Here, each radiation element is regarded as an individual source, and the triangular grid array is regarded as the isotropic point source array, as shown in Fig. 2.

The offsets of the two radiation element arrays are dx (equal to a in Fig. 1) in the x-direction and dy in the y-direction. By considering the radiation loss, the phase constant for m-order harmonic wave can be expressed as

$$\gamma = \beta_m - j \cdot \alpha \tag{3}$$

where j is the imaginary unit and α is the attenuation constant introduced by radiation. Therefore, the phase difference of the adjacent elements along x-direction can be written as

$$\delta = \gamma \cdot dx. \tag{4}$$

In this work, the beam directional pattern in $\varphi = 0$ plane is more concerned. According to the antenna array theory, the directional pattern can be calculated as

$$f_T(\theta) = \frac{\sin(M\psi)}{\sin(\psi)} + \frac{\sin[(M+1)\psi]}{\sin(\psi)} \tag{5}$$

where M presents the number of patch columns on both sides of the antenna, and ψ is given as

$$\psi = dx k_0 \sin\theta + \delta = dx(k_0 \sin\theta + \gamma). \tag{6}$$

To obtain a proper period p for the LWA radiation in the range of 6–12.3 GHz, it is necessary to analyze the relationship between the wavenumber β_m of space harmonics and the frequency f. According to (1), the radiation condition can be written as

$$-k_0 < \beta - \frac{2\pi}{p} < k_0. \tag{7}$$

It means that p should in the range

$$\frac{1}{\frac{\beta}{2\pi}+\frac{f}{c_0}} < p < \frac{1}{\frac{\beta}{2\pi}-\frac{f}{c_0}} \tag{8}$$

where c_0 is the light velocity in free space. By substituting the start and end frequencies f and their relative phase constant β into (8), the proper range of p is obtained.

III. Results and Discussion

A. Characteristics of the SSPP TL Based on Split-Ring Units

Before investigating the proposed LWA properties, we first study the characteristics of SSPP TL based on split-ring units. Fig. 3(a) shows the split-ring unit of the SSPP TL, which is composed of a central strip connected by two symmetric stubs with the width w_{stub} and the height h_{stub}, and two symmetric split-rings with the outer radius r_1, the inner radius r_2, and the gap angle Φ. The period of the unit is p_0 along the x-direction. The dispersion characteristics of this split-ring unit are simulated by using the Eigen mode solver of the CST Microwave Studio. The fundamental mode (mode I) dispersion curves for the split ring unit under different gap angle (Φ) are shown in Fig. 3(b). It is observed that all the dispersion curves deviate from the light line, which is similar to that of SPPs at optical frequencies. As the gap angle (Φ) decreases from 315°, 255°, 195°, 135°, 75° to 15°, the asymptotic frequency of the dispersion curve decreases from 50.13, 34.65, 24.22, 18.64, 14.56 to 12.54 GHz, respectively. Notably, the dispersion curve greatly deviates from the light line when $\Phi = 15°$, showing an extraordinary flatness feature when $\beta_x p_0/\pi > 0.5$. Generally, an SSPP TL with a lower dispersion curve possesses the characteristics of larger wave-vector β_x under a given operating frequency, larger phase difference for the same frequency change, and also shows stronger field confinement compared to an SSPP TL with a higher dispersion curve. Therefore, in this LWA design, the gap angle of the split unit in the SSPP TL in Section B is set as $\Phi = 15°$, and other dimension parameters are shown in Table I. Moreover, the dispersion curves for the first three modes of the split ring unit are also presented in Fig. 3(c). It is observed that the cutoff frequencies of the next two higher-order modes II and III are located at 12.3 and 24.5 GHz, respectively. Clearly, to achieve single-mode transmission, the operating frequency of the SSPP TL based on split-ring units should be lower than 12.3 GHz.

The characteristics of the whole SSPP TL are both simulated and experimentally verified. Fig. 4(a) shows the top-view and bottom-view of the SSPP TL, whose parameters are shown in Table I. Fig. 4(b) displays the comparison of the simulated and measured scattering parameters of the SSPP TL. The reflection coefficient S_{11} is lower than -10 dB and the transmission coefficient S_{21} is higher than -3 dB from 6.1 to 12.3 GHz, demonstrating a smooth conversion of the design from the quasi-TEM mode of microstrip to fundamental SSPP mode of the SSPP TL. Furthermore, a sharp roll-off with the cut-off frequency of 12.3 GHz is observed, which is close to the asymptotic frequency of 12.54 GHz for the fundamental mode dispersion curve of the split-ring unit shown in

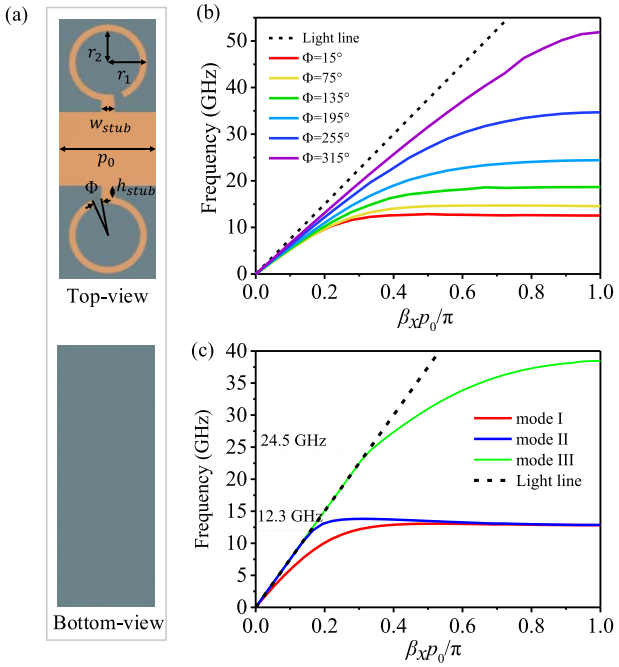

Fig. 3. Schematic and dispersion diagram of the split ring unit. (a) Top-view and bottom-view of the unit structure, (b) fundamental mode (mode I) dispersion diagram under different gap angle Φ, and (c) dispersion curves for the first three modes (modes I, II, and III) of the split ring unit. The detailed dimension parameters are listed in Table I.

Fig. 3(b) and (c). In general, the measured results are in good agreement with the simulation, while some minor deviations may result from the fabrication tolerance and impedance mismatching from the SMA connectors. To further study the propagation properties, the simulated near electric field $|E|$ distributions on $z = 0$ plane at 5, 7, 10.5, and 13.7 GHz are plotted in Fig. 4(c)–(f), respectively. It is observed that the EM waves propagate smoothly in the passband and the EM energy is bounded tighter with the frequency increasing as shown in Fig. 4(d) and (e). When the frequency is higher than 12.3 GHz, most of the EM energy is reflected, as shown in Fig. 4(f).

B. Properties of the SSPP LWA Based on Split-Ring Units

According to the previous discussion, the period p of radiation elements plays a critical role in the performance and operation band of the SSPP LWA. The range of the p value can be theoretically calculated by substituting the start and end frequencies and the corresponding phase constants obtained from the dispersion relation of the LWA into (8). It should be pointed out that the dispersion relations of the split-ring unit shown in Fig. 3(b) and (c) are obtained by using the Eigen mode solver by assuming that the SSPP TL is composed of infinite periodic units. However, the proposed LWA is based on a finite SSPP TL (Section B, 126 units) surrounded by two radiation patch arrays and connected two microstrip-SSPP TL transitions (Sections A and C). Therefore, it is not accurate enough to use the phase constants simply from the dispersion relation of the split-ring unit for the SSPP LWA period p calculation. Here, to be more accurate, we calculate the fundamental mode (mode I) dispersion relation for the SSPP LWA from simulated S-parameters by using the numerical

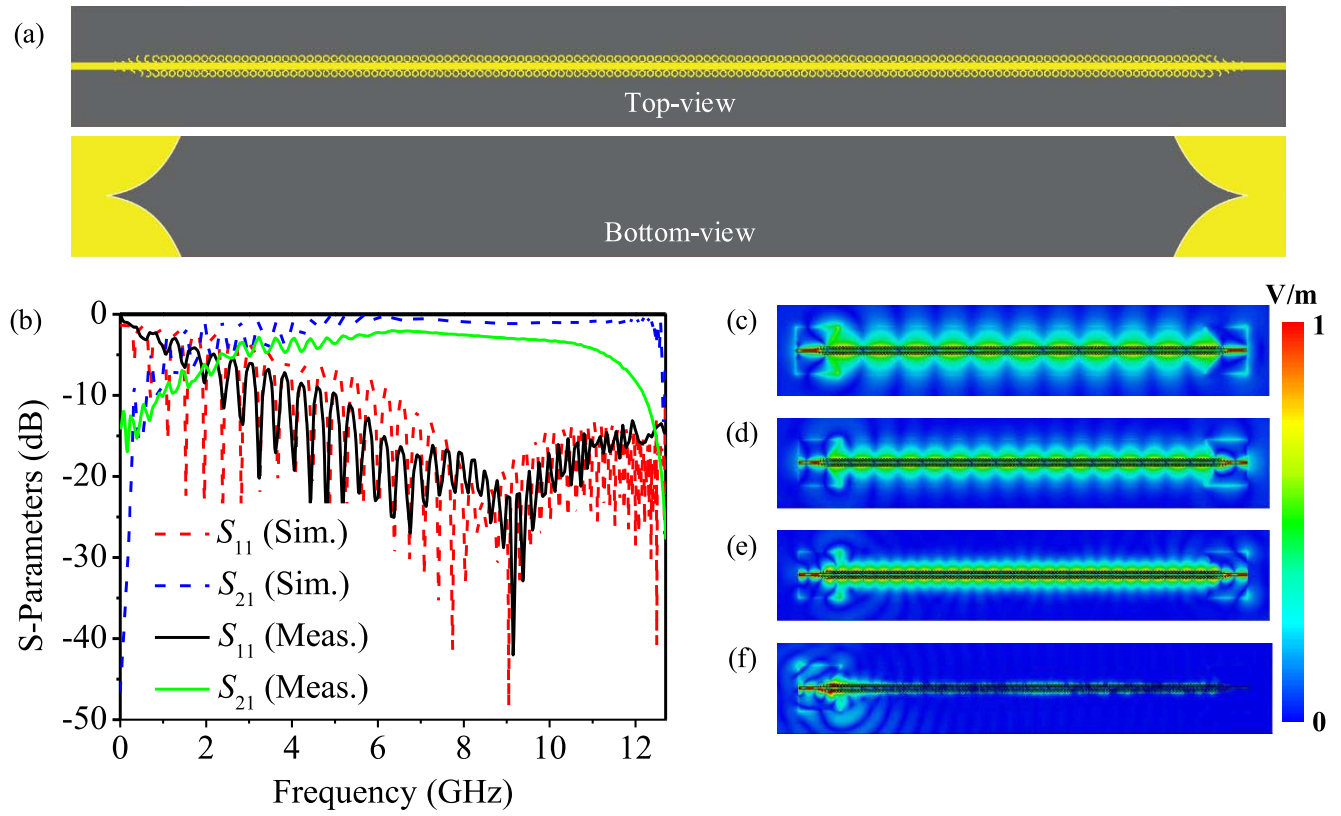

Fig. 4. Fabricated SSPP transmission line and the simulated and measured S-parameters of the proposed SSPP TL. (a) Top-view and bottom-view of the SSPP TL. (b) Simulated (dash lines) and the measured (solid lines) S-parameters of the proposed SSPP TL. (c)–(f) Simulated $|E|$ distribution at (c) 5 GHz, (d) 7 GHz, (e) 10.5 GHz, and 13.7 GHz in the $z = 0$ plane.

calibration method [41], as shown in Fig. 5(a). It is found that both dispersion curves, β_x versus frequency f, obtained from the finite-length structure calculated by the calibration method and from the infinite long structure simulated by the CST MWS Eigen mode solver have similar trends with a little difference. In 0–6 GHz, the calculated dispersion curve is slightly above the simulated dispersion curve. The calculated dispersion curve is below the simulated dispersion curve when the frequency is above 6 GHz. Although the difference between the two curves is not large, this difference will have a great impact on the antenna's frequency steering angle prediction. Considering the single-mode transmission passband of the SSPP TL shown in Figs. 3(c) and 4(b), we set the start and end steering frequencies of SSPP LWA at 6.3 and 12.2 GHz, respectively. From (8), we obtain that $19.8 < p < 21.4$ (unit: mm). In this work, we select $p = 20$ mm for the LWA design. Referring to (1), the dispersion relation of different space harmonic modes β_m ($m = 0, -1, -2$) versus f of the SSPP waveguide unit using the calibration method is shown in Fig. 5(b). It is found that $m = -1$ harmonic is located in the light cone in 6.3–12.2 GHz and the $m = -2$ harmonic is located in the light cone in 11–12.2 GHz range. To better indicate the dispersion characteristics of the proposed LWA, β_m/k_0 and the corresponding attenuation constant α/k_0 versus frequency f are further calculated in Fig. 5(c). The β_m/k_0 of the antenna in the fast-wave region is ranging from -1 to 1, which agrees well with those shown in Fig. 5(b). According to (2), the radiation beam angle is dependent on β_m/k_0.

As shown in Fig. 5(c), the $m = -1$ space harmonic entered in the fast-wave region from 6.27 to 12.22 GHz included the set start and end frequencies of 6.3 and 12.2 GHz, respectively. According to (2), theoretically, the radiated $m = -1$ harmonic wave can scan continuously from $-90°$ to $90°$ through broadside ($0°$ at about 9.5 GHz) from 6.27 to 12.22 GHz. However, it is worth noting that $m = -2$ order space harmonic wave enters the fast-wave region when the operation frequency is larger than 11 GHz. The presence of both -1 and -2 order harmonic waves will lead to the lobe of LWA split into two lobes (one main lobe generated by -1 order and the other side lobe generated by -2 order) in both backward and forward steering space in the frequency range 11–12.22 GHz. The generation of the secondary lobe will disperse the radiation energy and decrease the gain of the main lobe further. Thus, we mainly focus on $m = -1$ harmonic radiation performance of the LWA in this article. Fig. 5(c) also shows the calculated attenuation constant α for the LWA in the operating band. It is worth noting that unlike the propagation constant β_m, the attenuation constant α has only one curve. This is because the S-parameters cannot distinguish the relative contribution of the -1 and -2 modes, so the α extracted from the S-parameters can only be the superposition of all the effects of the fast mode radiation. It is noted that only the β_{-1} harmonic is in the fast-wave region in the 6.3–11 GHz

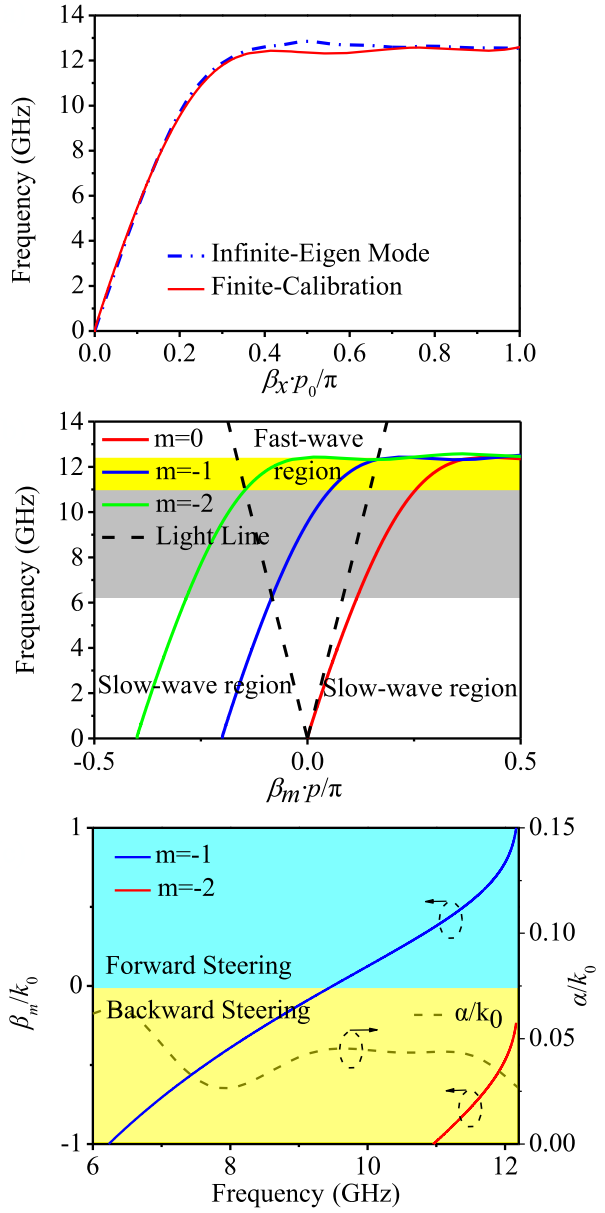

Fig. 5. Simulated and calculated dispersion curve of the split-ring unit and propagation constants of the proposed LWA versus frequency. (a) Fundamental mode dispersion curves ($\beta_x = \beta_0$) simulated by the infinite structure (Eigen mode) and calculated by the finite structure (calibration method), respectively. (b) Dispersion relation of different space harmonic modes β_m ($m = 0, -1, -2$) versus frequency f of the SSPP waveguide unit using the calibration method. (c) β_m/k_0 and α/k_0 versus frequency curves, respectively.

range, and α in this band can be considered to be entirely generated by the radiation of the β_{-1} harmonic. This constant presents the relation between directivity and frequency for aperture antenna. The bigger the α is, the shorter the equivalent radiation aperture is, leading to a wider beam and lower directional gain.

Fig. 6(a) shows the fabricated LWA prototype, where the detailed dimension parameters are shown in Figs. 1 and 3 and Table I. The simulated scattering parameters of the LWA are compared with measured results by an Agilent vector network analyzer, as shown in Fig. 6(b). It is clear that both

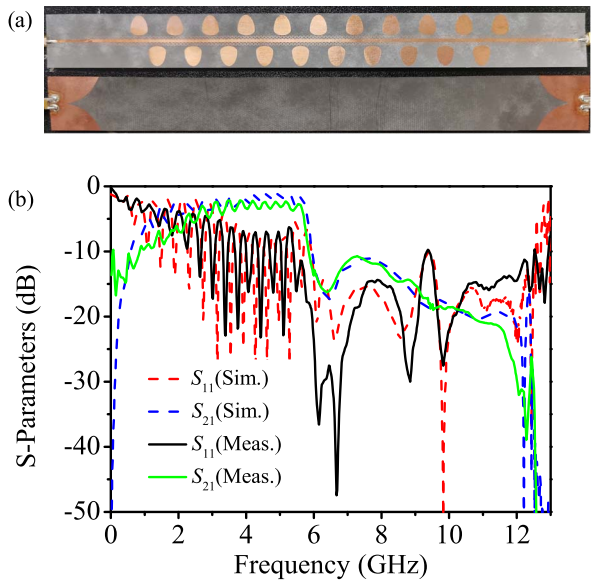

Fig. 6. Fabricated prototype and the simulated and measured S-parameters of the proposed LWA. (a) Top- and bottom-view of the antenna. (b) Simulated and measured S-parameters.

results are well matched over a wide range of frequencies. The transmission coefficient S_{21} and reflection coefficient S_{11} are lower than -10 dB from 6.3 to 12.2 GHz, indicating the power is radiated to the free space efficiently. The radiation efficiency of the proposed LWA, approximately evaluated by $1-|S_{11}|^2-|S_{21}|^2$, shows a minimal 90% in the whole radiation frequency band in 6.3–11 GHz.

Notably, optimization of the radiation patch shape of the proposed LWA may greatly improve the OSB effect suppression and enhance the radiation performance. Fig. 7(a) and (b) displays the structures of the proposed dual-half-elliptical patch and the common circular patch, where the radius and the distance of the circular patch are also set as r_x and g as the elliptical patch, respectively. Fig. 7(c) and (d) shows the surface current distributions of the dual half-elliptical patch and the circular patch under the same excitation. Clearly, the induced surface current on the bottom edge of the dual half-elliptical patch is stronger than the circular patch. Fig. 7(e) presents the comparison of simulated S-parameters of the antennas based on these two structures, respectively. Both S_{11} and S_{21} of the proposed antenna are lower than circular patch-loaded antenna in the operating band between 6.3 and 11 GHz. In particular, S_{11} around broadside frequency 9.5 GHz is 5 dB lowered by using the dual-half-elliptical patch structure, implying that the OSB effect near 9.5 GHz frequency is effectively suppressed. This is because the dual-half-elliptical patch has a smaller curvature and a longer effective coupling length in the x-direction, leading to tighter energy coupling between SSPP TL and the patches, and larger impedance variation near the patches loaded sections of the antenna. Therefore, by introducing the unique dual-half-elliptical radiation patches in the LWA design, the radiation efficiency is increased and the reflection is reduced simultaneously in the operating band.

To verify the above theoretical method, we simulate the whole LWA by using the Transient solver of CST MWS

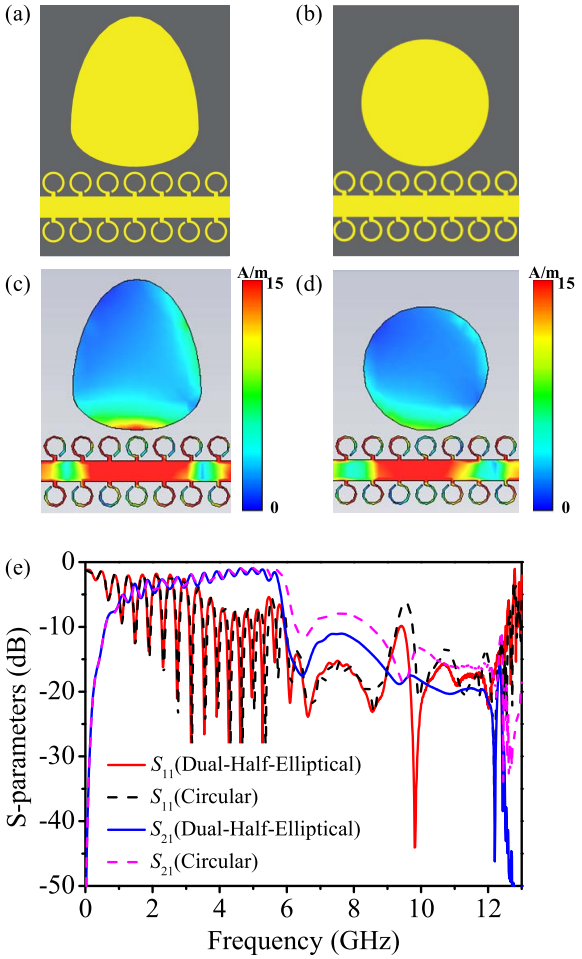

Fig. 7. Comparison of surface current (|J|) distributions and S-parameters affected by the proposed dual-half-elliptical patches and circular patches. (a) and (b) Dual-half-elliptical patch structure and circular patch structure, respectively. (c) and (d) Simulated surface current distributions on dual-half-elliptical patch and on circular patch, respectively. (e) Simulated S-parameters of the LWAs loaded with dual-half-elliptical patches and circular patches, respectively.

Studio. Fig. 8(a) presents the 11 GHz near-field distributions of the electric field ($|E|$) on the *xoy*-plane with $z = 0$ mm and the *xoz*-plane with $y = 0$ mm. It is found that the energy of surface waves decreases gradually along the x-direction and radiates into the free space. The simulated 3-D directional patterns at 6.3, 7.8, 9.5, and 11 GHz are plotted in Fig. 8(b)–(e) with a radiation angle $\theta_{-1} = -89°$, $-27°$, $-1°$ and $22°$, respectively. Since there is no ground plane in the radiation area of the LWA (see Section B), the LWA's radiation pattern is symmetric along the *xoy*-plane. From Fig. 8(b)–(e), it is observed that the radiation pattern along the elevation of the proposed antenna can be steered as the frequency sweeps and the scanning range could reach up to 112°. The gain of the antenna is changed with the operation frequency, and the variation trend is consistent with the attenuation constant shown in Fig. 5(c).

To further study the performance of the SSPP LWA, Fig. 9(a)–(d) shows the calculated, simulated, and measured normalized 2-D far-field radiation patterns in the $\varphi = 0$ plane of the designed LWA at different radiation frequencies of 6.3, 7.8, 9.5, and 11 GHz, respectively. It is worth noting that the θ ranging between $-90°$ and 90° represents the upper

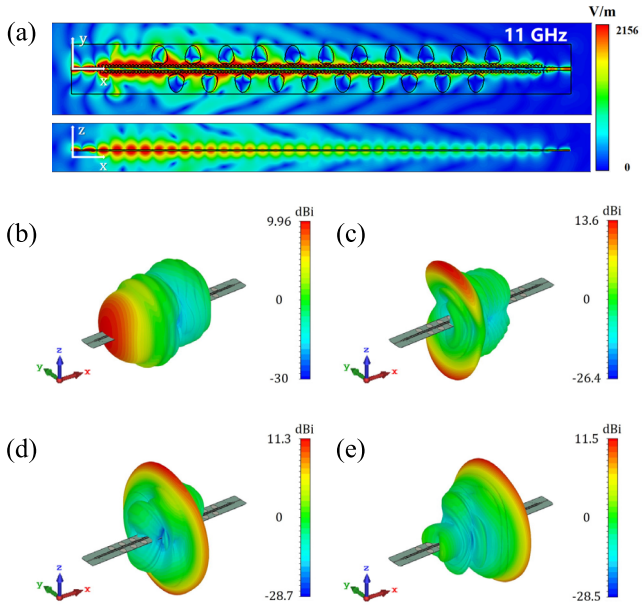

Fig. 8. Simulated near-field and far-field results of proposed LWA. (a) Simulated electric field ($|E|$) distribution on the top surface of the LWA at 11 GHz. (b)–(e) Three-dimensional far-field directional pattern of the proposed LWA at 6.3, 7.8, 9.5, and 11 GHz, respectively.

side of the *xoy*-plane, while the rest represents the lower region of the *xoy*-plane. The theoretical radiation pattern is calculated from (5) by using the phase constant β_{-1} and attenuation constant α shown in Fig. 5(b). In general, all three calculated, simulated, and measured radiation patterns and the main lobe directions are well matched, which verifies the accuracy and the effectivity of the theoretical method and model design of the SSPP LWA discussed above. However, it is worth noting that there are some tiny inconsistencies in the back lobe of these patterns. The simulated of the back-lobe pattern is closer to measurements than the calculated one in Fig. 9(a) and (d), while the calculated back-lobe pattern is closer to measurements than the simulated one in Fig. 9(b) and (c). This mismatch may be caused by the simplification of the calculation model, the simulation, and measurement error. In addition, the proposed LWA has a good polarization isolation performance with a very low cross-polarization level in the main lobe direction, as shown in Fig. 9(a)–(d). Although the cross-polarization level increases in the non-main lobe direction, it remains below -14 dB in all directions. Fig. 9(e) shows the calibrated calculated, simulated, and measured beam angle versus operation frequency with good agreement, implying that the beam steering characteristics of LWA is expected accurately. The main lobe of the SSPP LWA can be steering in a wide-angle range of 112° from back-fire ($-90°$) to the forward quadrant (22°) passing through the broadside direction and the sidelobe level is lower than -13 dB in the frequency range of 6.3–11 GHz, demonstrating a large scanning rate of 2.07°/%. According to Fig. 5(a), the dispersion curves of the finite-length structure extracted by the numerical calibration method are different from the dispersion curves of the infinite-length structure obtained by the simulation unit structure of CST MWS Eigen mode solver. To verify the accuracy of the dispersion curve extracted by

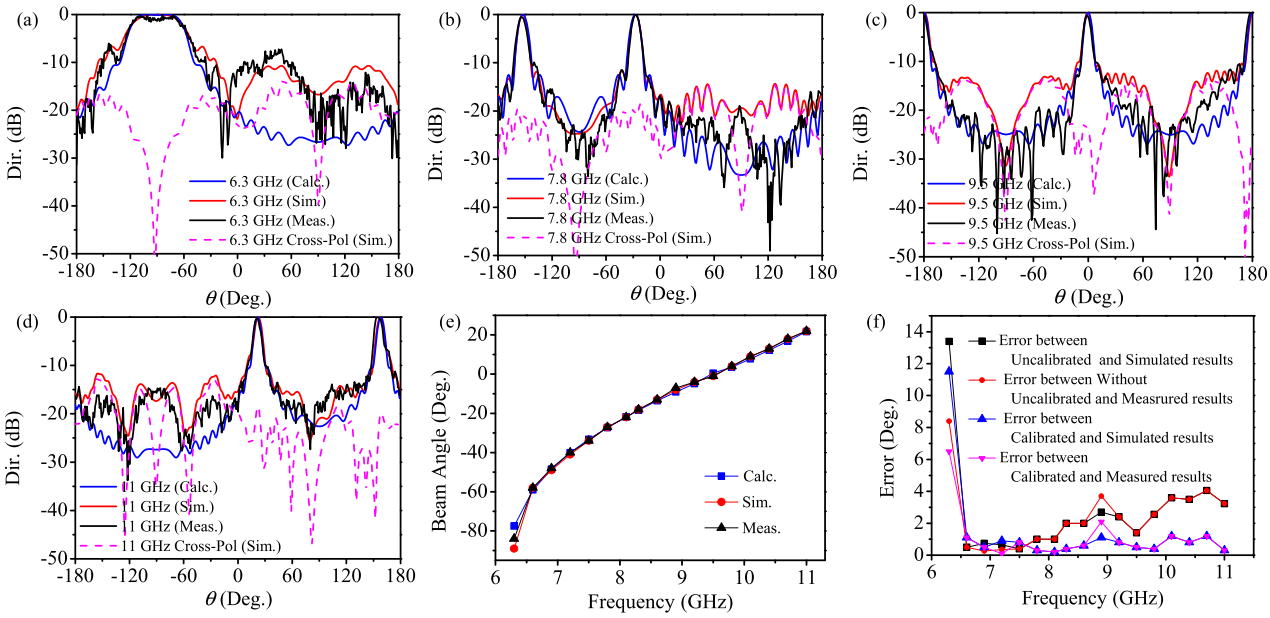

Fig. 9. Comparison of the calculated, simulated, and measured normalized far-field radiation patterns of the proposed LWA at different radiation frequencies: (a) 6.3 GHz, (b) 7.8 GHz, (c) 9.5 GHz, and (d) 11 GHz. (e) Comparison of the calculated, simulated, and measured main beam angle on the upper side of the *xoy*-plane [in the range from −90° to 90° range in Fig. 9(a)–(d)] versus operation frequency. (f) Comparison for the steering angle error between the dispersion curve obtained by CST MWS Eigen mode solver without numerical calibration and the dispersion curve extracted by the *S*-parameters obtained by CST MWS Transient solver with numerical calibration.

the calibration method, the finite-calibrated calculation curve and the uncalibrated infinite Eigen mode simulation dispersion curve were, respectively, used to calculate the scanning angle of the antenna. Fig. 9(f) displays the comparison for the steering angle error obtained from the dispersion curve with and without numerical calibration with respect to the simulated and experimental results. It is observed that the beam angle around 6.3 GHz calculated by both calibrated and uncalibrated dispersion curves are relatively large. When the frequency is higher than 6.3 GHz, the average error of the beam angle using the calibrated dispersion curve is about 0.7°, which is much smaller than that of 2° for the uncalibrated dispersion curve.

Furthermore, we also investigate the dual-beam radiation performance of the SSPP LWA. From the LWA dispersion relation shown in Fig. 5(c), the beam will split into two lobes in the range from −90° to 90° in 11–12.2 GHz, which are generated by the $m = -1$ and $m = -2$ space harmonic waves. We present the simulated and measured radiation patterns at 11.3 and 11.6 GHz in Fig. 10(a) and (b), respectively. As expected, the directions of the main dual-lobe of radiation patterns are in good agreement. Since the low efficiency of $m = -2$ space harmonic wave, the level of side lobes is much lower than the main lobes, especially in the experimental results. This phenomenon confirms the accuracy of the theoretical prediction.

Fig. 11 shows the simulated and measured gain and radiation efficiency versus operation frequency of the designed SSPP LWA. It simulated and measured results show that the SSPP LWA has excellent radiation performance with high efficiency over 90% (average of 95%), high gain ranging from 9 to 14.2 dBi (average of 12 dBi), and low sidelobe level (<−13 dB) in the whole operating band from 6.3 to 11 GHz. The gain is higher than 12 dBi in the backward steering band ranging from 7.2 to 9.5 GHz. However, the gain

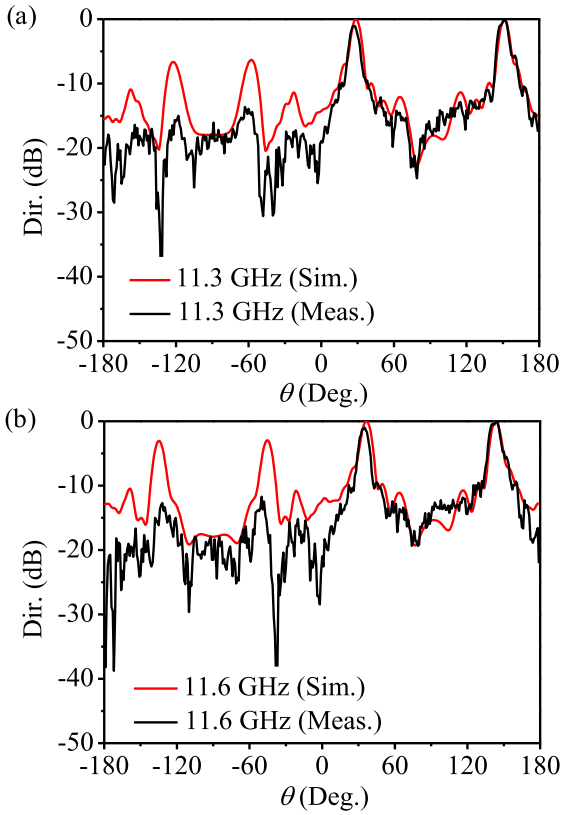

Fig. 10. Simulated and measured directional patterns in two beams band. (a) and (b) Simulated and measured directional patterns at 11.3 and 11.6 GHz, respectively.

reduced because of the wide beam width introduced by a large attenuation rate in 6.3–7.2 and 9.5–11 GHz bands.

Finally, the performance comparison of the proposed SSPP LWA with some recently reported LWAs is presented

TABLE II
COMPARISON OF THE PROPOSED SSPP LWA WITH OTHER REPORTED WORKS

Reference Works	LWA Length	Scanning Range (Degree)	Bandwidth (GHz)	Relative Bandwidth	Average Efficiency	Implementation Technique	Scanning Rate (°/%)	Average Gain (dBi)
[7]	$14\lambda_g$	88(-50~+38)	5.9(8.4~14.3)	52%	80%	SIW-Slotted	1.69	12.2
[11]	$11.86\lambda_g$	55(-35~+20)	3(6-9)	40%	75%	Patch Loaded	1.38	9.8
[27]	$29.93\lambda_g$	152(no data)	2.2(8.5~10.7)	23%	67%	Patch Loaded	6.6	9
[28]	$10.87\lambda_g$	123(-60~63)	1(10.6~11.6)	9%	40.2%	SIW-Slotted	13.7	7.9
[30]	N/A	18(-10~+8)	1.3(8.5~9.8)	14%	N/A	CRLH	1.28	15
[31]	$31.87\lambda_g$	90(-45~+45)	16(8~24)	100%	N/A	Patch Loaded	0.9	12.5
[36]	$19.91\lambda_g$	59(-69~-10)	7.2(22~29.2)	33%	N/A	SIW-Slotted	1.78	16.2
[39]	$14.65\lambda_g$	60(-54-6)	5(11-16)	37%	N/A	Patch Loaded	1.62	12
[42]	$8.46\lambda_g$	27(no data)	0.2(2.4~2.6)	8%	80%	Stub-slotted	3.3	5.6
[43]	$4.89\lambda_g$	97(-42~55)	2.5(-9~11.5)	23.8%	95%	SIW-Slotted	4.1	9.6
[44]	$4\lambda_g$	128(-66~62)	N/A	N/A	50%	CRLH CPWG with-varactors	N/A	5-9.9
This work	$14\lambda_g$	112(-90~+22)	4.7(6.3~11)	54%	95%	Patch Loaded	2.07	12

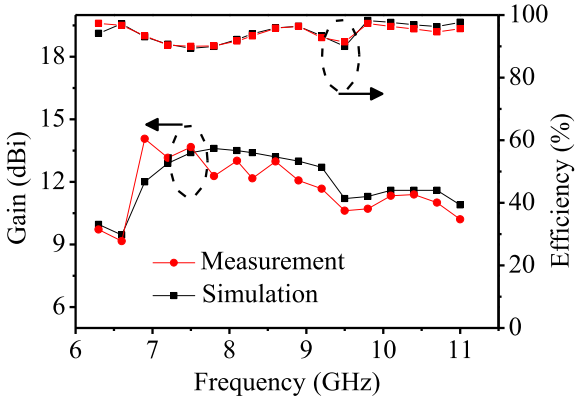

Fig. 11. Simulated and measured gain and efficient of the proposed LWA.

in Table II. To better evaluate the performances of the proposed LWAs, many key radiation parameters including compactness, scanning range, scanning rate, average efficiency, average gain, ease of design and implementation should be considered in the comparison. It is found that even though one or some specific parameters might be somewhat worse than other works because of various factors like different waveguide types or radiation mechanisms, the proposed SSPP LWA demonstrates superior or at least competitive overall performance over the other LWAs. The advantages of the proposed SSPP LWA mainly contain a relatively compact size, a wide scanning range of 112° covering the back-fire radiation, a high average gain of 12 dBi, a high average efficiency of 95%, and a high scanning rate (2.07°/%). Besides, unlike the LWAs based on SIWs in [28], [36], and [43] and CRLH CPWG with-varactors in [44], the proposed SSPP LWA does not require metallization through holes and complicated biasing circuits, which may somehow ease the antenna implementation.

IV. CONCLUSION

In this article, we demonstrate an efficient back-fire to forward wide-angle beam steering LWA based on a large dispersion gradient planar SSPP TL with split ring units. To interpret the mechanism and precisely predict the radiation pattern of the LWA, an accurate theoretical method combined with the numerical calibrated dispersion relation for the SSPP TL is proposed. In the LWA design, two arrays of combined half-elliptical patches are periodically arranged on either side of the SSPP TL to improve the radiation performance and reduce the open-stopband effect. To validate the proposed design, both SSPP TL and LWA prototypes were fabricated and measured. The theoretical calculation, numerical simulation, and experimental results are in good agreement and show that the proposed SSPP LWA has good radiation performances. The main beam of the LWA can switch from back-fire (−90°) to forward quadrant (22°) in the wide side direction of 6.3–11 GHz, showing a large scanning range of 112° and a high scanning rate of 2.07°/%. The proposed LWA possesses high gain (average 12 dBi) and low sidelobe level (<−13 dB), which may find great potential in the development of microwave radar and wireless communication systems.

REFERENCES

[1] A. A. Oliner and A. Hessel, "Guided waves on sinusoidally-modulated reactance surfaces," *IRE Trans. Antennas Propag.*, vol. 7, no. 5, pp. 201–208, 1959.
[2] A. Sutinjo, M. Okoniewski, and R. H. Johnston, "Radiation from fast and slow traveling waves," *IEEE Antennas Propag. Mag.*, vol. 50, no. 4, pp. 175–181, Aug. 2008.
[3] D. R. Jackson, C. Caloz, and T. Itoh, "Leaky-wave antennas," *Proc. IEEE*, vol. 100, no. 7, pp. 2194–2206, Jul. 2012.
[4] Y. Li, Q. Xue, E. K.-N. Yung, and Y. Long, "The periodic half-width microstrip leaky-wave antenna with a backward to forward scanning capability," *IEEE Trans. Antennas Propag.*, vol. 58, no. 3, pp. 963–966, Mar. 2010.
[5] G.-F. Cheng and C.-K. C. Tzuang, "A differentially excited coupled half-width microstrip leaky EH_1 mode antenna," *IEEE Trans. Antennas Propag.*, vol. 61, no. 12, pp. 5885–5892, Dec. 2013.
[6] J. Liu, D. R. Jackson, and Y. Long, "Substrate integrated waveguide (SIW) leaky-wave antenna with transverse slots," *IEEE Trans. Antennas Propag.*, vol. 60, no. 1, pp. 20–29, Jan. 2012.
[7] D. K. Karmokar, S.-L. Chen, D. Thalakotuna, P.-Y. Qin, T. S. Bird, and Y. J. Guo, "Continuous backward-to-forward scanning 1-D slot-array leaky-wave antenna with improved gain," *IEEE Antennas Wireless Propag. Lett.*, vol. 19, no. 1, pp. 89–93, Jan. 2020.
[8] L. Liu, C. Caloz, and T. Itoh, "Dominant mode leaky-wave antenna with backfire-to-endfire scanning capability," *Electron. Lett.*, vol. 38, no. 23, pp. 1414–1416, Nov. 2002.
[9] X.-L. Tang *et al.*, "Continuous beam steering through broadside using asymmetrically modulated Goubau line leaky-wave antennas," *Sci. Rep.*, vol. 7, no. 1, p. 8, Sep. 2017.
[10] K. Rudramuni *et al.*, "Goubau-line leaky-wave antenna for wide-angle beam scanning from backfire to endfire," *IEEE Antennas Wireless Propag. Lett.*, vol. 17, no. 8, pp. 1571–1574, Aug. 2018.
[11] J. Y. Yin *et al.*, "Frequency-controlled broad-angle beam scanning of patch array fed by spoof surface plasmon polaritons," *IEEE Trans. Antennas Propag.*, vol. 64, no. 12, pp. 5181–5189, Dec. 2016.

[12] B. Ren, W. Li, Z. Qin, Y. Wang, L. Zhang, and B. Zhang, "Leaky wave antenna based on periodically truncated SSPP waveguide," *Plasmonics*, vol. 15, no. 2, pp. 551–558, Apr. 2020.
[13] J. B. Pendry, L. Martín-Moreno, and F. J. Garcia-Vidal, "Mimicking surface plasmons with structured surfaces," *Science*, vol. 305, no. 5685, pp. 847–848, Aug. 2004.
[14] A. P. Hibbins, B. R. Evans, and J. R. Sambles, "Experimental verification of designer surface plasmons," *Science*, vol. 308, no. 5722, pp. 670–672, Apr. 2005.
[15] S. A. Maier, S. R. Andrews, L. Martín-Moreno, and F. J. García-Vidal, "Terahertz surface plasmon-polariton propagation and focusing on periodically corrugated metal wires," *Phys. Rev. Lett.*, vol. 97, no. 17, p. 4, Oct. 2006.
[16] C. R. Williams, S. R. Andrews, S. A. Maier, A. I. Fernández-Domínguez, L. Martín-Moreno, and F. J. García-Vidal, "Highly confined guiding of terahertz surface plasmon polaritons on structured metal surfaces," *Nature Photon.*, vol. 2, no. 3, pp. 175–179, Mar. 2008.
[17] X. Shen, T. J. Cui, D. F. Martin-Cano, and J. Garcia-Vidal, "Conformal surface plasmons propagating on ultrathin and flexible films," *Proc. Nat. Acad. Sci. USA*, vol. 110, no. 1, pp. 40–45, Jan. 2013.
[18] Z. Liao, J. Zhao, B. C. Pan, X. P. Shen, and T. J. Cui, "Broadband transition between microstrip line and conformal surface plasmon waveguide," *J. Phys. D, Appl. Phys.*, vol. 47, no. 31, Aug. 2014, Art. no. 315103.
[19] L. Liu *et al.*, "Multi-channel composite spoof surface plasmon polaritons propagating along periodically corrugated metallic thin films," *J. Appl. Phys.*, vol. 116, no. 1, Jul. 2014, Art. no. 013501.
[20] X. Liu, Y. Feng, K. Chen, B. Zhu, J. Zhao, and T. Jiang, "Planar surface plasmonic waveguide devices based on symmetric corrugated thin film structures," *Opt. Exp.*, vol. 22, no. 17, pp. 20107–20116, Aug. 2014.
[21] L. Ye, Y. Chen, Z. Wang, C. Zhu, J. Zhuo, and Q. H. Liu, "Compact spoof surface plasmon polariton waveguides and notch filters based on meander-strip units," *IEEE Photon. Technol. Lett.*, vol. 33, no. 3, pp. 135–138, Feb. 1, 2021.
[22] L. Ye *et al.*, "Super subwavelength guiding and rejecting of terahertz spoof SPPs enabled by planar plasmonic waveguides and notch filters based on spiral-shaped units," *J. Lightw. Technol.*, vol. 36, no. 20, pp. 4988–4994, Oct. 15, 2018.
[23] H. C. Zhang, S. Liu, X. Shen, L. H. Chen, L. Li, and T. J. Cui, "Broadband amplification of spoof surface plasmon polaritons at microwave frequencies," *Laser Photon. Rev.*, vol. 9, no. 1, pp. 83–90, Jan. 2015.
[24] L. Ye, H. Feng, W. Li, and Q. H. Liu, "Ultra-compact spoof surface plasmon polariton waveguides and notch filters based on double-sided parallel-strip lines," *J. Phys. D, Appl. Phys.*, vol. 53, no. 26, Jun. 2020, Art. no. 265502.
[25] L. Ye, Y. Chen, J. Zhou, H. Feng, Y. Zhang, and Q. H. Liu, "High-performance spoof surface plasmon polariton waveguides and splitters based on Greek-cross fractal units," *J. Phys. D, Appl. Phys.*, vol. 53, no. 23, Jun. 2020, Art. no. 235502.
[26] H. Feng, L. Ye, Y. Zhang, W. Li, H. Chen, and Q. H. Liu, "Bidirectional multi-mode microwave vortex beam generation enabled by spoof surface plasmon polaritons," *Appl. Phys. Lett.*, vol. 117, no. 24, Dec. 2020, Art. no. 241601.
[27] G. Zhang, Q. Zhang, Y. Chen, and R. D. Murch, "High-scanning-rate and wide-angle leaky-wave antennas based on glide-symmetry Goubau line," *IEEE Trans. Antennas Propag.*, vol. 68, no. 4, pp. 2531–2540, Apr. 2020.
[28] S. Xu *et al.*, "A wide-angle narrowband leaky-wave antenna based on substrate integrated waveguide-spoof surface plasmon polariton structure," *IEEE Antennas Wireless Propag. Lett.*, vol. 18, no. 7, pp. 1386–1389, Jul. 2019.
[29] J. J. Xu, H. C. Zhang, Q. Zhang, and T. J. Cui, "Efficient conversion of surface-plasmon-like modes to spatial radiated modes," *Appl. Phys. Lett.*, vol. 106, no. 2, Jan. 2015, Art. no. 021102.
[30] G. S. Kong, H. F. Ma, B. G. Cai, and T. J. Cui, "Continuous leaky-wave scanning using periodically modulated spoof plasmonic waveguide," *Sci. Rep.*, vol. 6, no. 1, p. 9, Jul. 2016.
[31] L. L. Liu, J. Wang, X. X. Yin, and Z. N. Chen, "Wide-angle beam scanning leaky-wave antenna using spoof surface plasmon polaritons structure," *Electronics*, vol. 7, no. 12, p. 11, Dec. 2018.
[32] X. Du, H. Li, and Y. Yin, "Wideband fish-bone antenna utilizing odd-mode spoof surface plasmon polaritons for endfire radiation," *IEEE Trans. Antennas Propag.*, vol. 67, no. 7, pp. 4848–4853, Jul. 2019.
[33] W. Ma, W. Cao, S. Shi, and X. Yang, "Compact high gain leaky-wave antennas based on substrate integrated waveguide TE_{220} mode," *IEEE Access*, vol. 7, pp. 145060–145066, 2019.
[34] Y. Han, J. Wang, Y. Li, S. Gong, J. Zhang, and S. Qu, "A frequency-scanning antenna based on hybridization of the quasi-TEM mode and spoof surface plasmon polaritons mode," *J. Phys. D, Appl. Phys.*, vol. 52, no. 38, Sep. 2019, Art. no. 38LT01.
[35] H. Jiang *et al.*, "Backward-to-forward wide-angle fast beam-scanning leaky-wave antenna with consistent gain," *IEEE Trans. Antennas Propag.*, vol. 69, no. 5, pp. 2987–2992, May 2021.
[36] Y. Lin, Y. Zhang, H. Liu, Y. Zhang, E. Forsberg, and S. He, "A simple high-gain millimeter-wave leaky-wave slot antenna based on a bent corrugated SIW," *IEEE Access*, vol. 8, pp. 91999–92006, 2020.
[37] D.-F. Guan, P. You, Q. Zhang, Z.-H. Lu, S.-W. Yong, and K. Xiao, "A wide-angle and circularly polarized beam-scanning antenna based on microstrip spoof surface plasmon polariton transmission line," *IEEE Antennas Wireless Propag. Lett.*, vol. 16, pp. 2538–2541, 2017.
[38] X. Lv, W. Cao, Z. Zeng, and S. Shi, "A circularly polarized frequency beam-scanning antenna fed by a microstrip spoof SPP transmission line," *IEEE Antennas Wireless Propag. Lett.*, vol. 17, no. 7, pp. 1329–1333, Jul. 2018.
[39] A. Q. Zhu *et al.*, "Compact spoof surface plasmon polariton leaky-wave antenna with consistent gain," *Microw. Opt. Technol. Lett.*, vol. 63, no. 9, pp. 2430–2435, Sep. 2021.
[40] R. T. Yan *et al.*, "A broadband and high-efficiency compact transition from microstrip line to spoof surface plasmon polaritons," *IEEE Microw. Wireless Compon. Lett.*, vol. 30, no. 1, pp. 23–26, Jan. 2020.
[41] F. Xu and K. Wu, "Numerical multimode calibration technique for extraction of complex propagation constants of substrate integrated waveguide," in *IEEE MTT-S Int. Microw. Symp. Dig.*, vol. 2, Jun. 2004, pp. 1229–1232.
[42] G. Zhang, Q. Zhang, S. Ge, Y. Chen, and R. D. Murch, "High scanning-rate leaky-wave antenna using complementary microstrip-slot stubs," *IEEE Trans. Antennas Propag.*, vol. 67, no. 5, pp. 2913–2922, May 2019.
[43] S.-L. Chen, D. K. Karmokar, Z. Li, P.-Y. Qin, R. W. Ziolkowski, and Y. J. Guo, "Circular-polarized substrate-integrated-waveguide leaky-wave antenna with wide-angle and consistent-gain continuous beam scanning," *IEEE Trans. Antennas Propag.*, vol. 67, no. 7, pp. 4418–4428, Jul. 2019.
[44] S. Xie, J. Li, G. Deng, J. Feng, and S. Xiao, "A wide-angle scanning leaky-wave antenna based on a composite right/left-handed transmission line," *Appl. Sci.*, vol. 10, no. 6, p. 1927, Mar. 2020.

Longfang Ye (Member, IEEE) received the Ph.D. degree in electromagnetic field and microwave technology from the University of Electronic Science and Technology of China, Chengdu, China, in 2013.

From October 2011 to January 2013, he was a Visiting Student with the Massachusetts Institute of Technology, Cambridge, MA, USA. From November 2019 to October 2020, he was a Visiting Professor with the Bionanophotonics Systems Laboratory, École Polytechnique Fédérale de Lausanne, Lausanne, Switzerland. He is currently an Associate Professor with the Institute of Electromagnetics and Acoustics, Xiamen University, Xiamen, China, and the Shenzhen Research Institute, Xiamen University, Shenzhen, China, and the State Key Laboratory of Millimeter Waves, Southeast University, Nanjing, China. He has published over 100 papers in peer-reviewed journals and conference proceedings. His current research interests include microwave and terahertz waveguides, circuits, and antennas, plasmonics, metamaterials, and graphene-based devices.

Dr. Ye has served as a Reviewer for several journals, including the *Nanoscale*, *Carbon, Advanced Optical Materials*, *Laser & Photonics Reviews*, *Journal of Lightwave Technology*, *Optics Express*, *New Journal of Physics*, IEEE MICROWAVE AND WIRELESS COMPONENTS LETTERS, IEEE ANTENNAS AND WIRELESS PROPAGATION LETTERS, the IEEE TRANSACTIONS ON VEHICULAR TECHNOLOGY, IEEE PHOTONICS JOURNAL, *Scientific Reports*, IEEE ACCESS, IEEE PHOTONICS TECHNOLOGY LETTERS, *ACS Applied Materials & Interfaces*, *ACS Omega*, *Applied Optics*, *Photonic Sensors*, *Applied Physics A*, *International Journal of Numerical Modelling: Electronic Networks, Devices and Fields*, *Microwave and Optical Technology Letters*, *International Journal of RF and Microwave Computer-Aided Engineering*, and *Engineering Research Express*.

Zhengyi Wang was born in Beijing, China, in 1996. He received the B.Eng. degree in information engineering from Northwestern Polytechnical University, Xi'an, Shaanxi, China, in 2019. He is currently pursuing the M.Eng. degree in electromagnetics and microwave technology with Xiamen University, Xiamen, Fujian, China.

His current research interests include spoof surface plasmon polaritons and leaky-wave antennas.

Jianliang Zhuo (Member, IEEE) received the B.S. degree in communication engineering and business administration and the M.S. degree in communication and information system from the University of Electronic Science and Technology of China, Chengdu, China, in 2007 and 2011, respectively, and the Ph.D. degree in physical electronics from Xiamen University, Xiamen, China, in 2018.

Since 2018, he has been a Post-Doctoral Fellow with the Postdoctoral Mobile Station of Information and Communication Engineering, Xiamen University. His research interests include fast forward solvers in electromagnetics and inverse scattering methods for microelectronics and RF systems.

Feng Han (Senior Member, IEEE) received the B.S. degree in electronic science from Beijing Normal University, Beijing, China, in 2003, the M.S. degree in geophysics from Peking University, Beijing, in 2006, and the Ph.D. degree in electrical engineering from Duke University, Durham, NC, USA, in 2011.

Since July 2015, he has been with Xiamen University, Xiamen, China, where he is currently an Associate Professor of the Institute of Electromagnetics and Acoustics. He has published over 50 articles in refereed journals. His research interests include electromagnetic scattering and inverse scattering in complex media, fast full-wave electromagnetic inversion based on machine learning, configuration of the antenna array for electromagnetic inverse problems, and geophysical electromagnetic exploration and inversion.

Weiwen Li (Senior Member, IEEE) received the B.S. degree in electronic engineering from Jilin University, Changchun, China, in 1993, and the M.S. degree in material engineering and the Ph.D. degree in electronic engineering from Zhejiang University, Hangzhou, China, in 2002 and 2005, respectively.

He is currently an Associate Professor of electronic engineering with Xiamen University, Xiamen, China. His research interests include electromagnetic field theory, antenna technology, electromagnetic metamaterials, and microwave technology.

Qing Huo Liu (Fellow, IEEE) received the B.S. and M.S. degrees in physics from Xiamen University, Xiamen, China, in 1983 and 1986, respectively, and the Ph.D. degree in electrical engineering from the University of Illinois at Urbana-Champaign, Champaign, IL, USA, in 1989.

He was a Research Assistant with the Electromagnetics Laboratory, University of Illinois at Urbana Champaign, from September 1986 to December 1988, where he was a Post-Doctoral Research Associate from January 1989 to February 1990. He was a Research Scientist and the Program Leader of Schlumberger-Doll Research, Ridgefield, CT, USA, from 1990 to 1995. From 1996 to May 1999, he was an Associate Professor with New Mexico State University, Las Cruces, NM, USA. Since June 1999, he has been with Duke University, Durham, NC, USA, where he is currently a Professor of electrical and computer engineering. His research interests include computational electromagnetics and acoustics, inverse problems, and their application in nanophotonics, geophysics, biomedical imaging, and electronic design automation. He has published widely in these areas.

Dr. Liu is also a fellow of the Acoustical Society of America, the Electromagnetics Academy, and the Optical Society of America. He received the 1996 Presidential Early Career Award for Scientists and Engineers (PECASE) from the White House, the 1996 Early Career Research Award from the Environmental Protection Agency, the 1997 Career Award from the National Science Foundation, the 2017 Technical Achievement Award and the 2018 Computational Electromagnetics Award from the Applied Computational Electromagnetics Society, and the 2018 Harrington-Mittra Award in Computational Electromagnetics from the IEEE Antennas and Propagation Society. In 2018, he also received the University of Illinois at Urbana-Champaign ECE Distinguished Alumni Award. He has served as the founding Editor-in-Chief for the IEEE JOURNAL ON MULTISCALE AND MULTIPHYSICS COMPUTATIONAL TECHNIQUES. He has also served as an IEEE Antennas and Propagation Society Distinguished Lecturer.